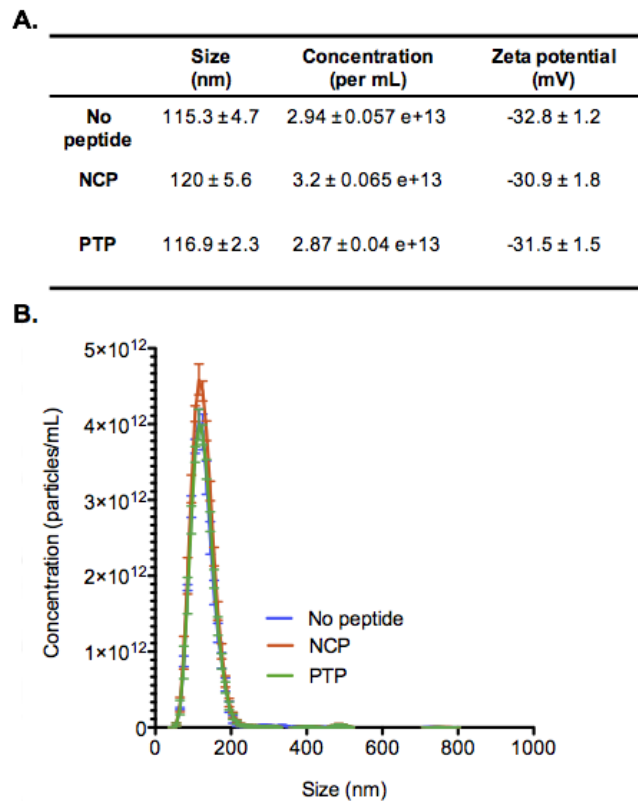
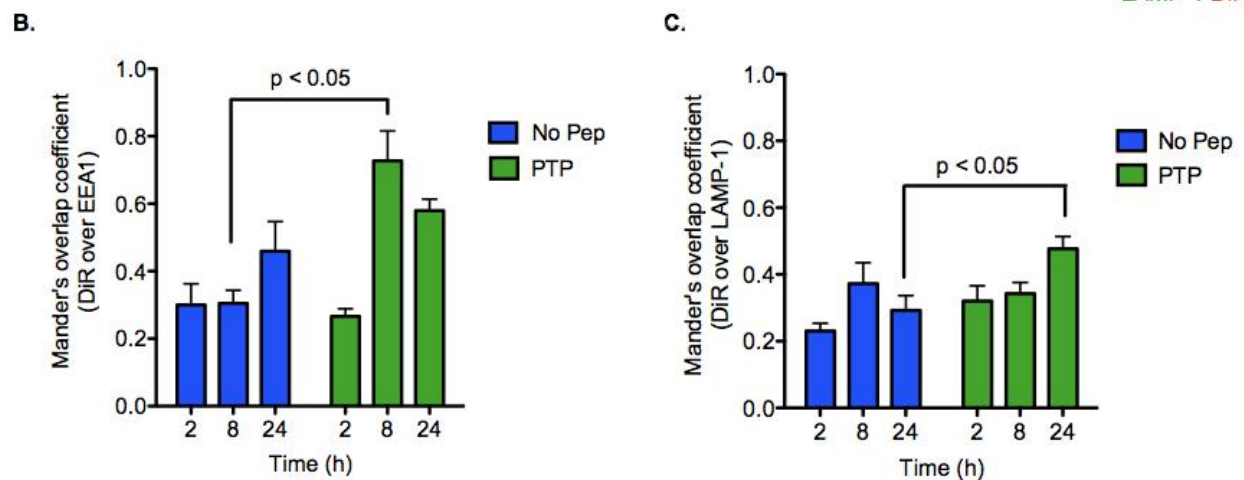
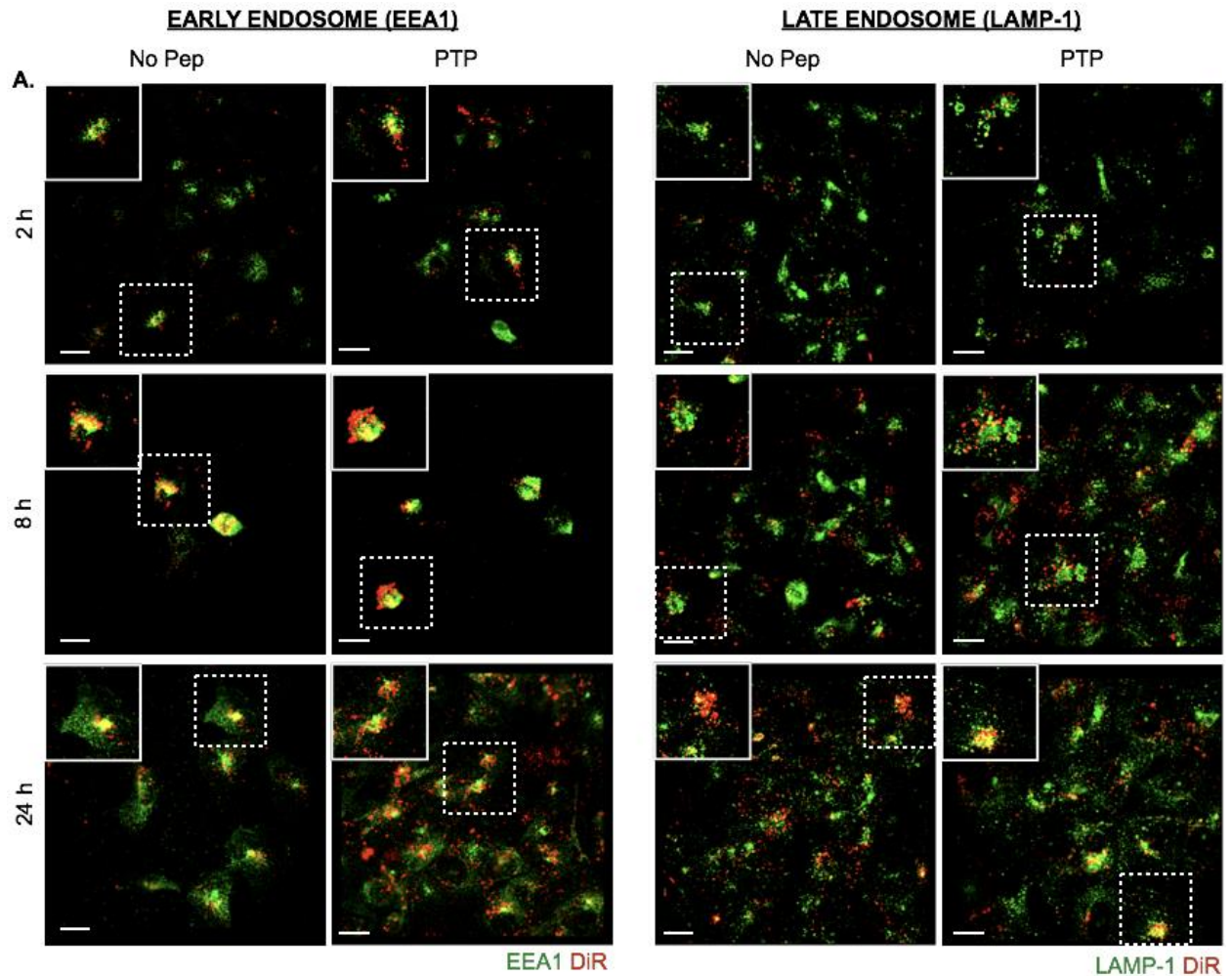


Supplementary Figures for Dasa et al. "Plectin-targeted liposomes enhance the therapeutic efficacy of a PARP inhibitor in the treatment of ovarian cancer"



**Figure S1. Liposome characterization using NanoSight and Zetasizer. (A)** Table showing the size, concentration and zeta potential of no peptide, NCP and PTP liposomes. The three liposomal formulations did not vary a lot in terms of size and concentration, the size ranged from 115-120 nm and concentration from 2.87-3.2 e+13 / mL. The Zeta potential was also comparable between the no peptide, NCP and PTP liposomes that was about -31 to -33 mV. **(B)** Graph showing the size and concentration distribution of no peptide, NCP and PTP liposomes.



**Figure S2. OVCAR8 cells endocytose PTP liposomes. (A)** Confocal microscopy of liposomal DiR (red), early (EEA1-green) and late endosomal markers (LAMP-1-green) show No Pep and PTP liposomes are taken up by OVCAR8 cells by endocytosis. (Scale bar; 10  $\mu$ m). **(B)** Mander's overlap coefficient (DiR/ EEA1) for No Pep and PTP liposomes at 2, 8, and 24h after incubation. **(C)** Mander's overlap coefficient (DiR/ LAMP-1) for No Pep and PTP liposomes at 2, 8, and 24h after incubation.

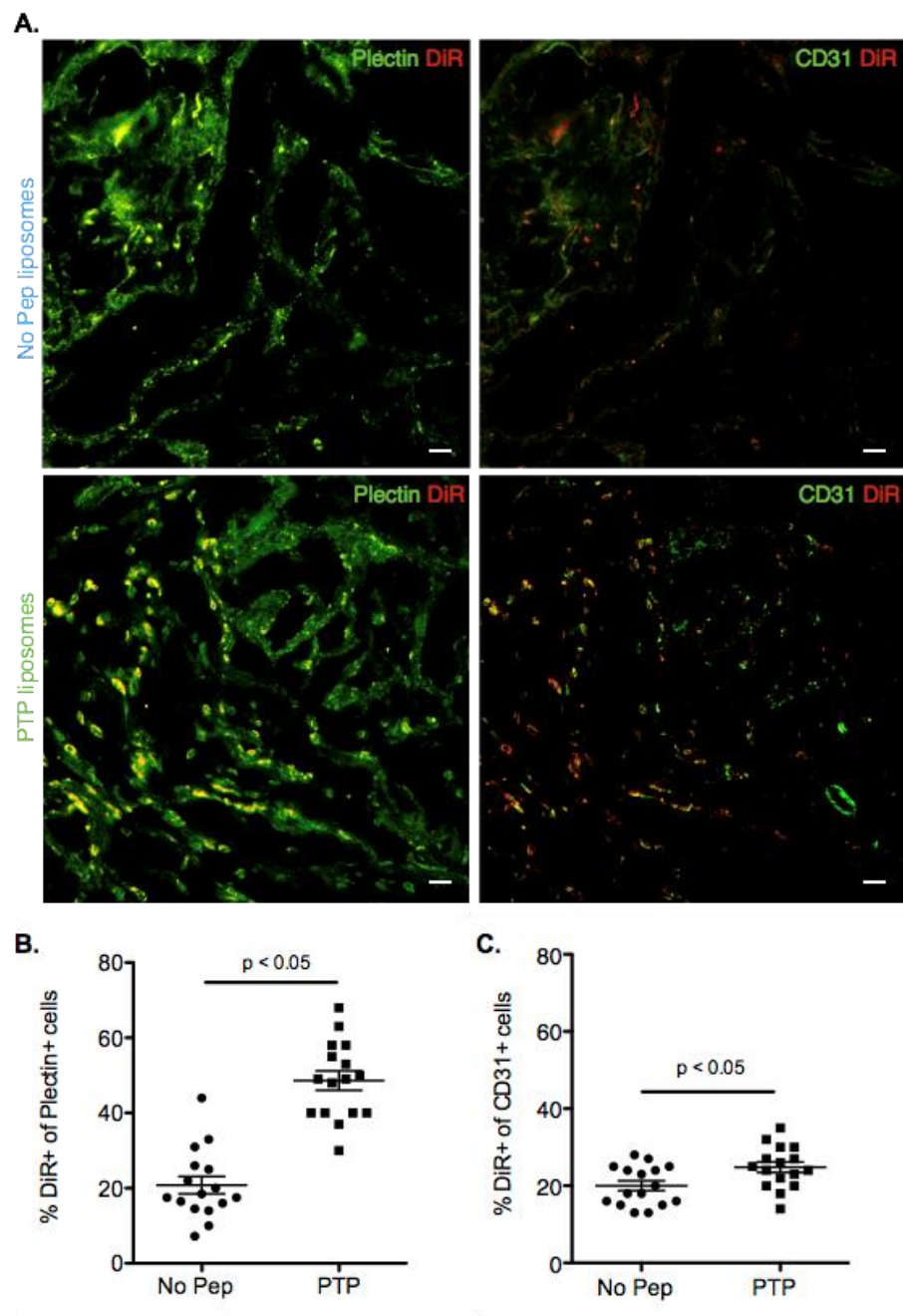
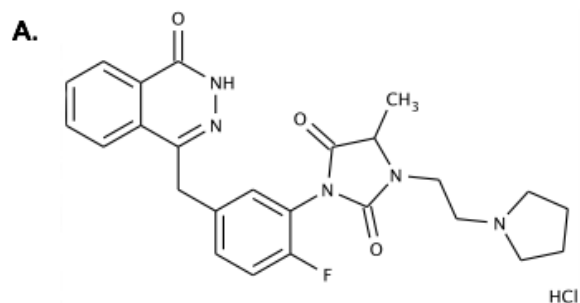


**Figure S3. PTP liposomes associate with plectin+ tumor cells.** (A) Immunofluorescence of (left) liposomal DiR (red) vs. plectin (green) and (right) liposomal DiR (red) vs. CD31 (green) demonstrates that liposomes (red) were associated with plectin+ (green) and CD31+ (green) endothelial cells. (Scale bar; 20  $\mu$ m). (B) Liposomal DiR association with plectin+ tumor cells was determined by ImageJ and represented as %DiR+ of plectin+ cells. (C) Similarly, Liposomal DiR association with CD31+ endothelial cells was determined by ImageJ and represented as %DiR+ of CD31+ cells.



**B.**

Properties	AZ7379
pKa	11.5a, 8.7a, 8.94c
Polar surface area A <sup>2</sup>	85.32b
Total Area A <sup>2</sup>	667.06b
Non-polar area A <sup>2</sup>	587.74b
Non-polar/polar	6.818b
Solubility (mM) [pH]	2.5[7.4]c
Charge [pH]	1.02 [5,6,7,7.4]b
pI	9.72b
Log P	1.89a,2.75a
LogD at pH 7	1.05a
t <sub>1/2</sub> - Oral (min)	55.6
t <sub>1/2</sub> - i.v (min)	3.4

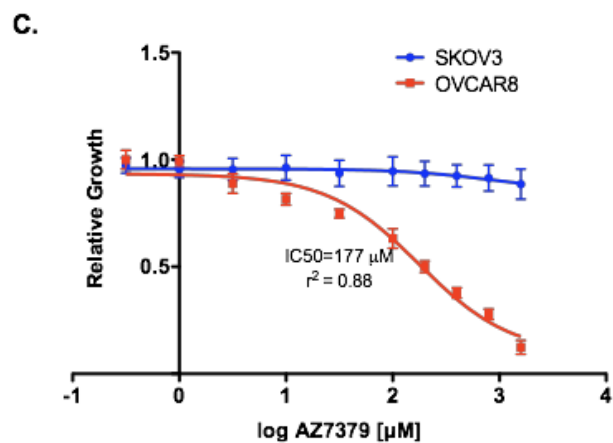


**Figure S4. Physicochemical properties of AZ7379 and *in vitro* inhibition of PARP-1. (A)** Structure of AZ7379 **(B)** Physical and Chemical properties of AZ7379. **(C)** *In vitro* growth inhibition assay in SKOV3 and OVCAR8 cells.

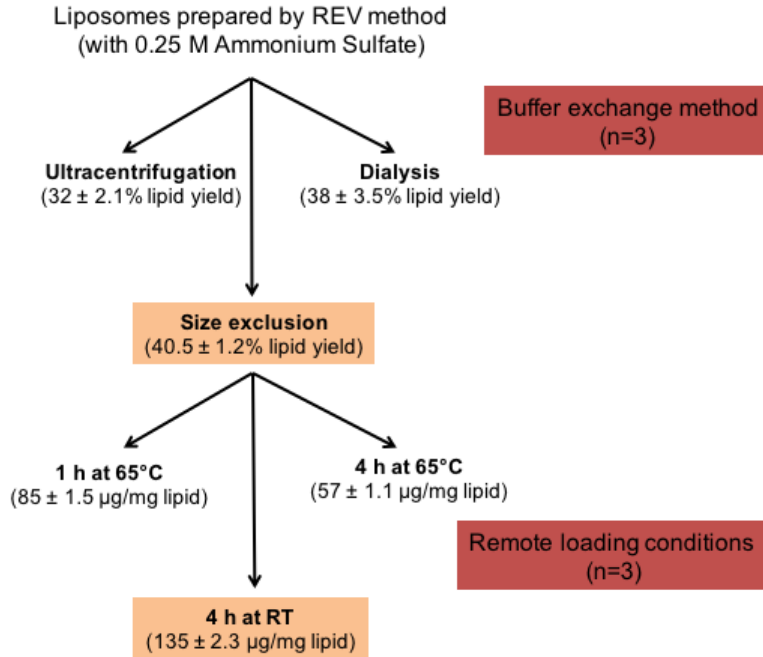


**Figure S5. Steps involved in the optimization of AZ7379 remote loading.** First step in optimizing remote loading was to identify the buffer exchange method with the least loss of lipid (compare ultracentrifugation, size exclusion and dialysis) followed by determining the optimum condition for maximum encapsulation of AZ7379 (65°C for 1h or 4h and 4h at room temperature).

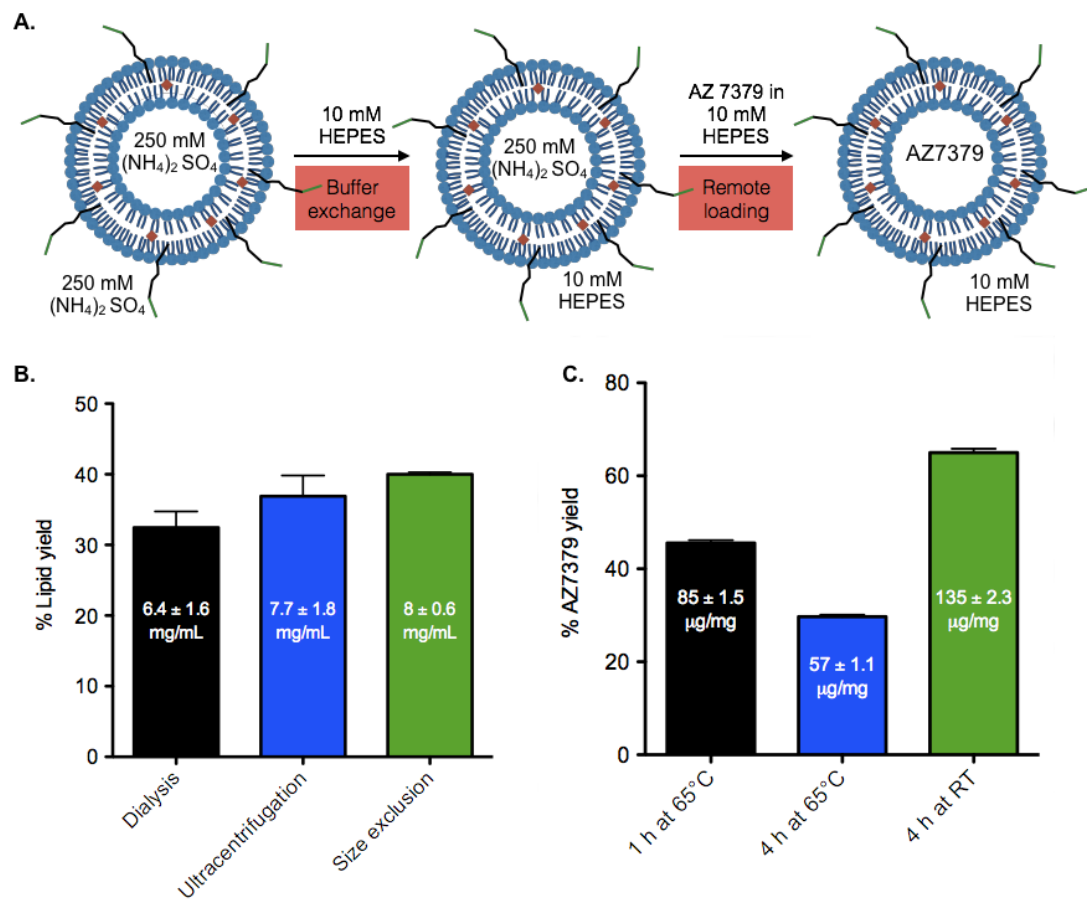


**Figure S6. Remote loading of AZ7379.** (A) Schematics of remote loading using peptide conjugated liposomes. (B) Graph showing the percentage of lipid recovered via three buffer exchange methods - dialysis, ultracentrifugation and size exclusion. Maximum yield was obtained by the size exclusion method and although ultracentrifugation yielded similar lipid recovery, liposomes resuspended into buffer eventually precipitated suggesting instability in this process. The values inside the bars represents final lipid concentration (mg/mL). (C) Graph showing percentage of AZ7379 remote loaded using three different conditions - 1 h at 65°C, 4 h at 65°C and 4h at RT. Maximum AZ7379 yield was achieved with 4h at RT. The values inside the bars represent final drug to lipid ratio (µg/mg).

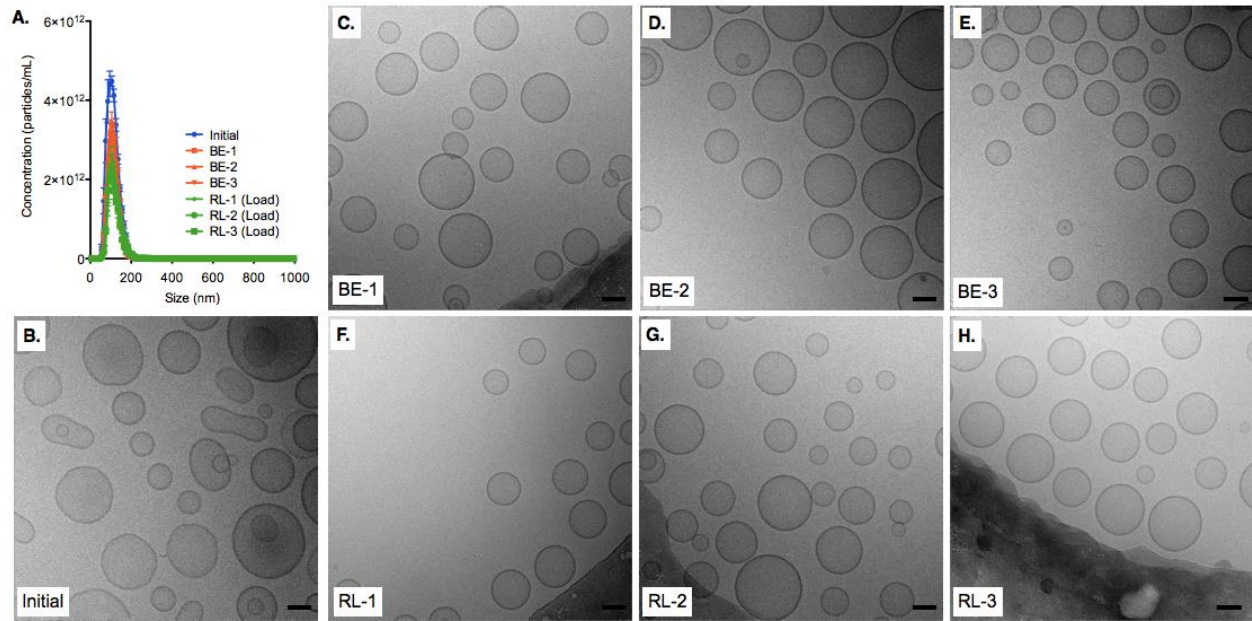


**Figure S7. NanoSight and TEM analysis of liposomes at various stages of AZ7379 remote loading. (A)** Graph showing size and concentration of liposomes in initial preparation, 3 aliquots undergoing gel filtration (size exclusion) to remove excess ammonium sulfate (BE= buffer exchange, BE-1, BE-2, BE-3 in triplicate) and remote loaded liposomes that have undergone another gel filtration step to remove unloaded AZ7379 (RL= remote loading, RL-1, RL-2, RL-3 in triplicate). Images of liposomes from various stages of remote loading obtained using cryo-TEM. **(B)** Initial liposome preparation containing ammonium sulfate inside and outside of liposomes. **(C-E)** Liposomes after buffer exchange (BE-1, BE-2 and BE-3) and **(F-H)** after remote loading of AZ7379. (Scale bar; 50 nm).

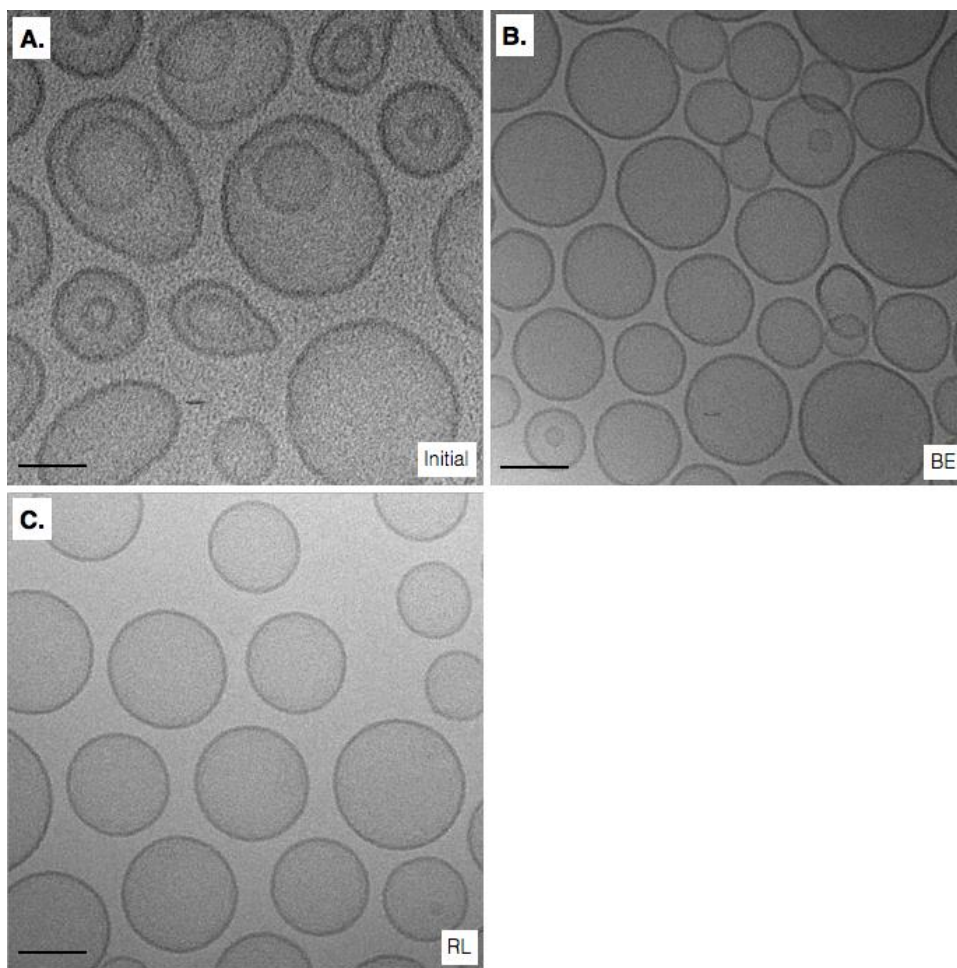


**Figure S8. TEM analysis of PTP liposomes at various stages of AZ7379 remote loading. (A-C)** TEM of liposomes during remote loading (initial, BE, and RL) suggest there was no considerable change in their structure during remote loading process. (BE – buffer exchange, RL – remote loaded liposomes) (Scale bar; 50 nm).

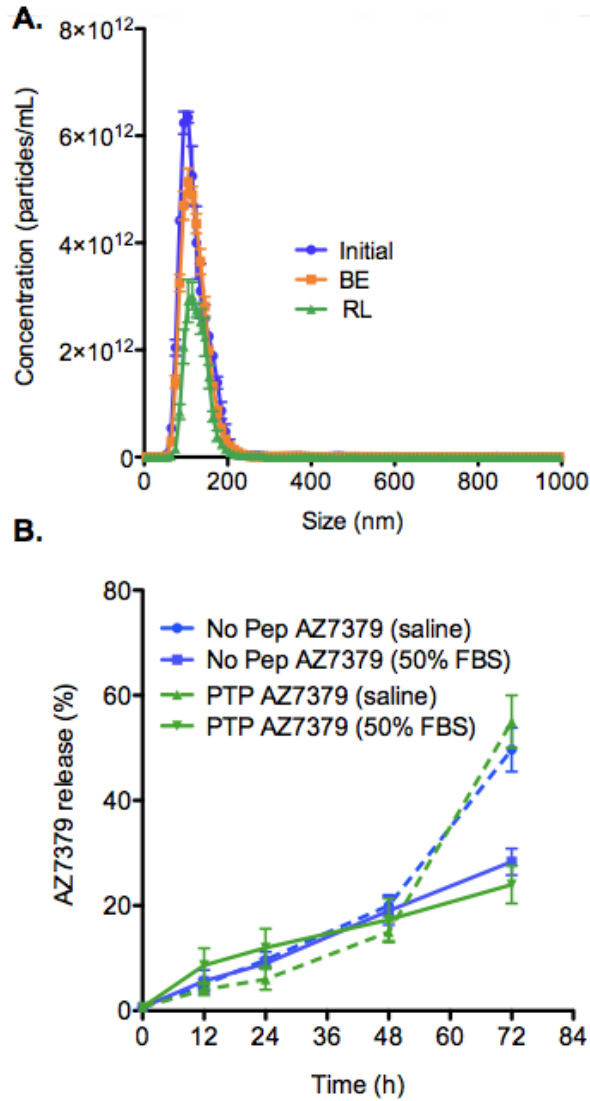
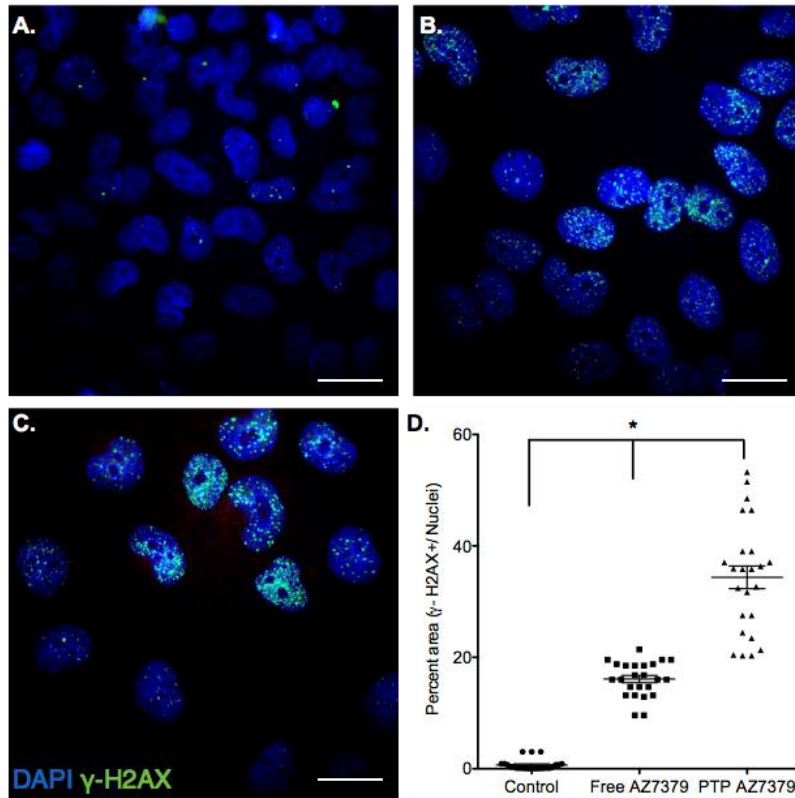


**Figure S9. NanoSight analysis of PTP liposomes during remote loading and AZ7379 release *in vitro*.** (A) Graph showing the size and concentration of PTP liposomes at various stages of remote loading (Initial, BE- buffer exchange to remove ammonium sulfate and RL- AZ7379 remote loaded PTP liposomes). (B) Graph showing AZ7379 in saline and 50% FBS from liposomes (No Pep and PTP) with time.

## AZ7379 induces ds-DNA breaks



## AZ7379 causes trapping of PARP-1

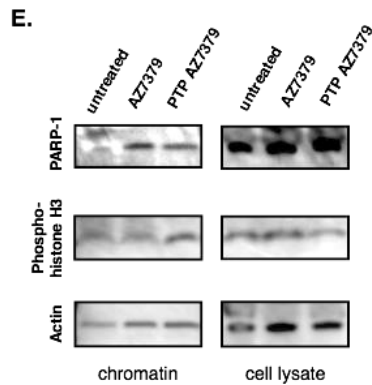


**Figure S10. AZ7379 causes ds-DNA breaks and also traps PARP-1 on chromatin.** Double stranded (ds)- DNA breaks were visualized by confocal microscopy after immunostaining for  $\gamma$ -H2AX (green) and nucleus (DAPI) in (A) untreated, (B) free AZ7379 and (C) PTP AZ7379 treated OVCAR8 cells.  $\gamma$ -H2AX indicates the presence of DNA breaks. (Scale bar; 10  $\mu$ m). (D) ds-DNA breaks were quantified by measuring the percent nuclear area that was also  $\gamma$ -H2AX+. (E) The extent of PARP-1 trapping on chromatin in OVCAR8 cells *in vitro* was analyzed via Western blot.

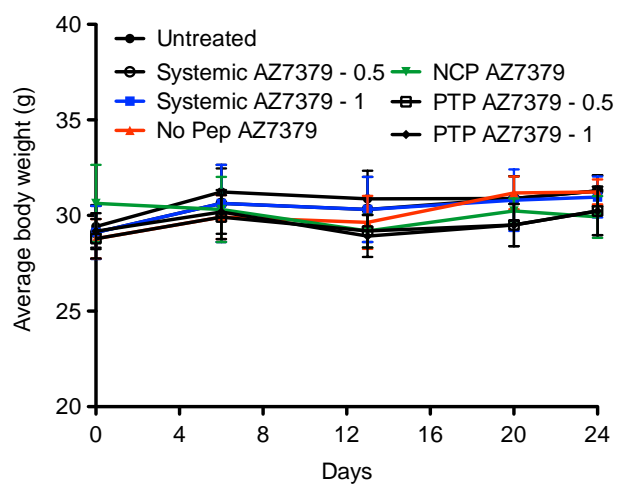


**Figure S11. Average body weights of mice during the tumor growth studies.** Average body weight of mice from all the groups during the treatment process was not significantly different in the treatment groups.

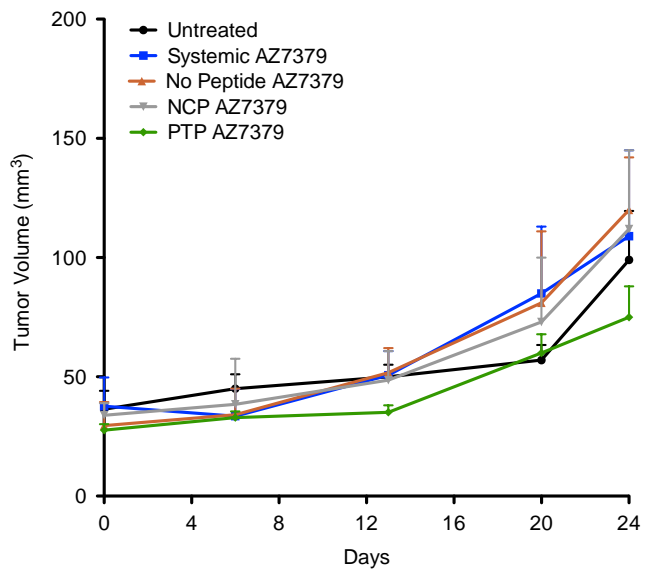


**Figure S12. SKOV3 tumor volume in response to AZ7379 delivery.** Tumor volume (mm<sup>3</sup>) was measured every week following treatment and plotted over time to determine the efficacy of each treatment group. PTP liposomes loaded with AZ7379 were not effective in preventing tumor growth compared to other groups.

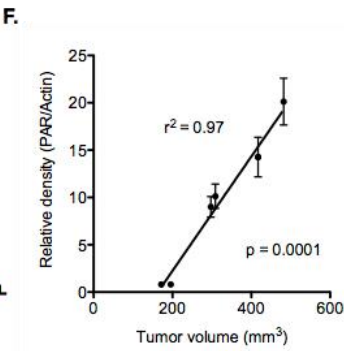
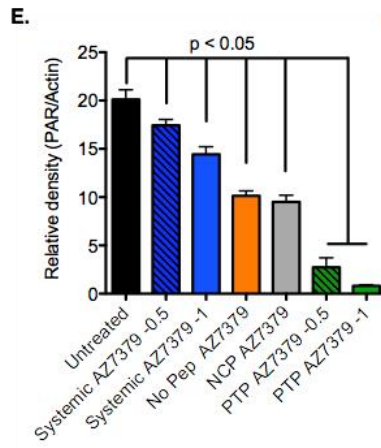
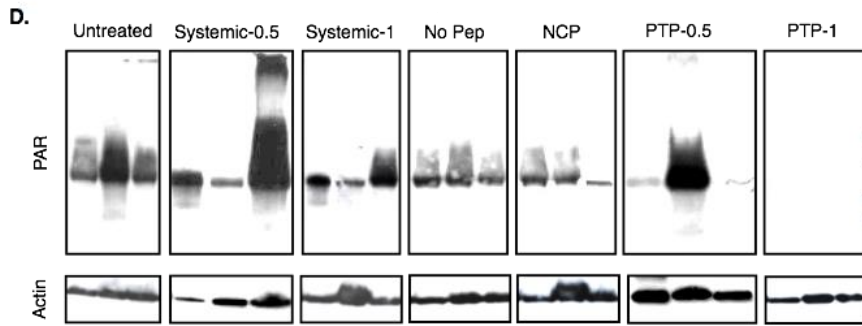
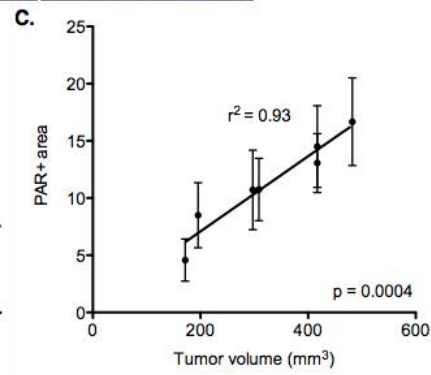
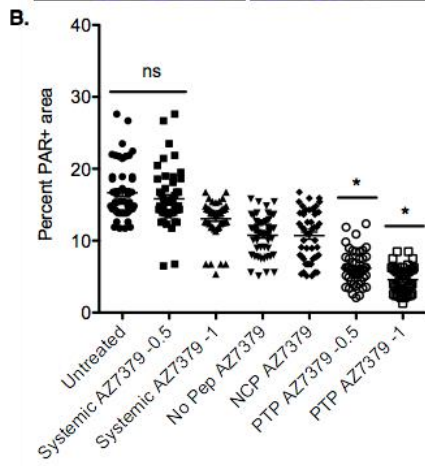
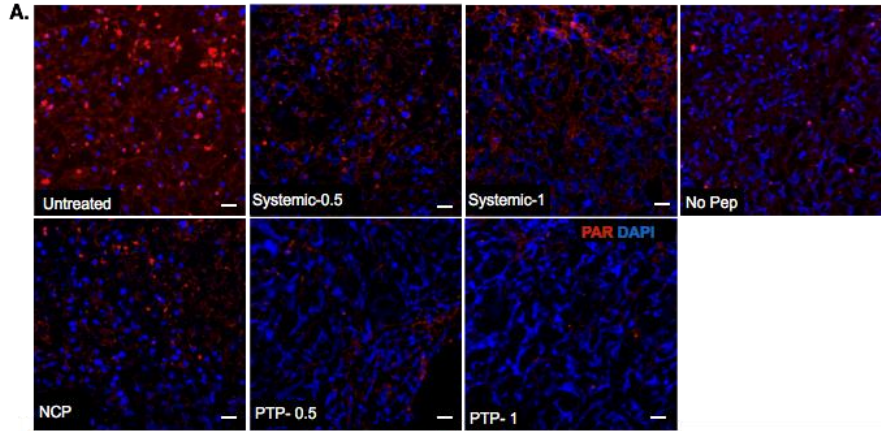


**Figure S13. PAR quantification in OVCAR8 tumors by immunofluorescence and Western blot. (A)** PAR immunofluorescence (red) in relation to cell nuclei stained with DAPI (blue) in tumor sections from 5 groups. PTP liposomes had lowest levels of PAR suggesting higher accumulation of AZ7379 in the tumor. **(B)** PAR was quantified using Image J from 10 images per tumor (4 at 20x and 6 and 60X magnification) and represented as percent PAR+ area. PTP liposomes had the least PAR+ area again confirming greater accumulation of AZ7379 in these tumors. (n.s – non significant) (\* represents  $p < 0.05$ ). **(C)** Correlation between tumor volume ( $\text{mm}^3$ ) by caliper measurements and percent PAR+ area through immunofluorescence. **(D)** PAR was also quantified from tumor lysates by Western blot. The Western blot images represents lysates from 3 animals of each group included in this study. PAR expression was normalized to actin expression in the same lysates/ blot. **(E)** Western blot quantification of PAR bands using densitometer readings normalized to actin levels in each sample and represented as relative density (PAR/Actin) (\* represents  $p < 0.05$ ). **(F)** Correlation between tumor volume ( $\text{mm}^3$ ) by caliper measurements and relative density (PAR/Actin) determined through Western blot and densitometry.

Background fluorescence (720 nm) in mice maintained on non-fluorescent diet

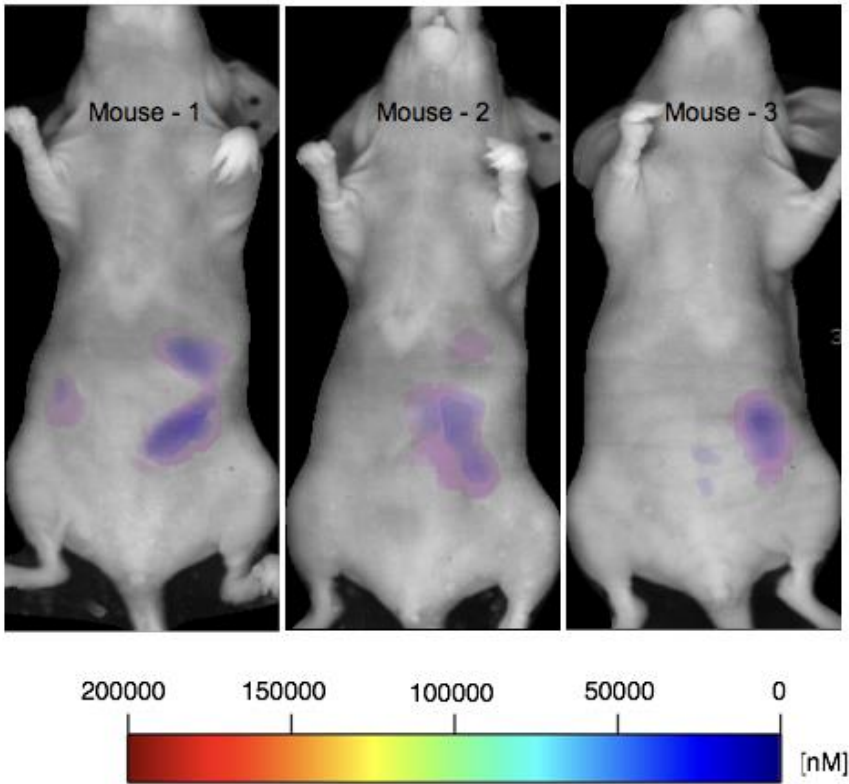


**Figure S14. Background fluorescence in mice maintained on non-fluorescent diet measured by FMT.** Mice were maintained on non-fluorescent diet for 10 days prior to tumor cell injection. FMT imaging was performed at the end of 10 days to observe the background fluorescent levels in the gut region. Based on the FMT quantification, there was minimal fluorescence in the 720 nm emission filter (0-2000 nM).

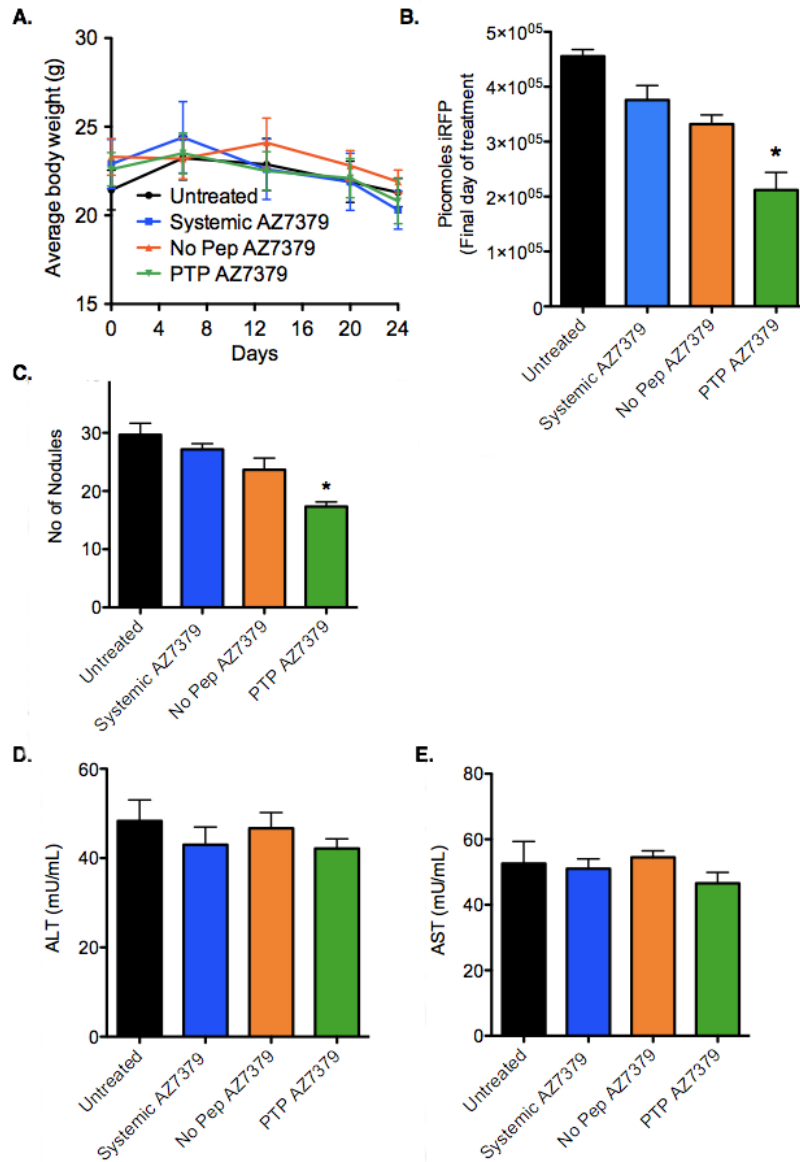


**Figure S15. PTP liposomes reduce tumor growth without inducing liver toxicity.** (A) Average body weight of mice from all the groups during the treatment process from different groups. (B) Average fluorescence of OVCAR8 tumors at the end of treatment. (C) Number of visible tumor nodules in the intraperitoneal cavity were counted and represented as average number of nodules per treatment group. Serum (D) ALT and (E) AST levels were quantified at the end of treatment period.

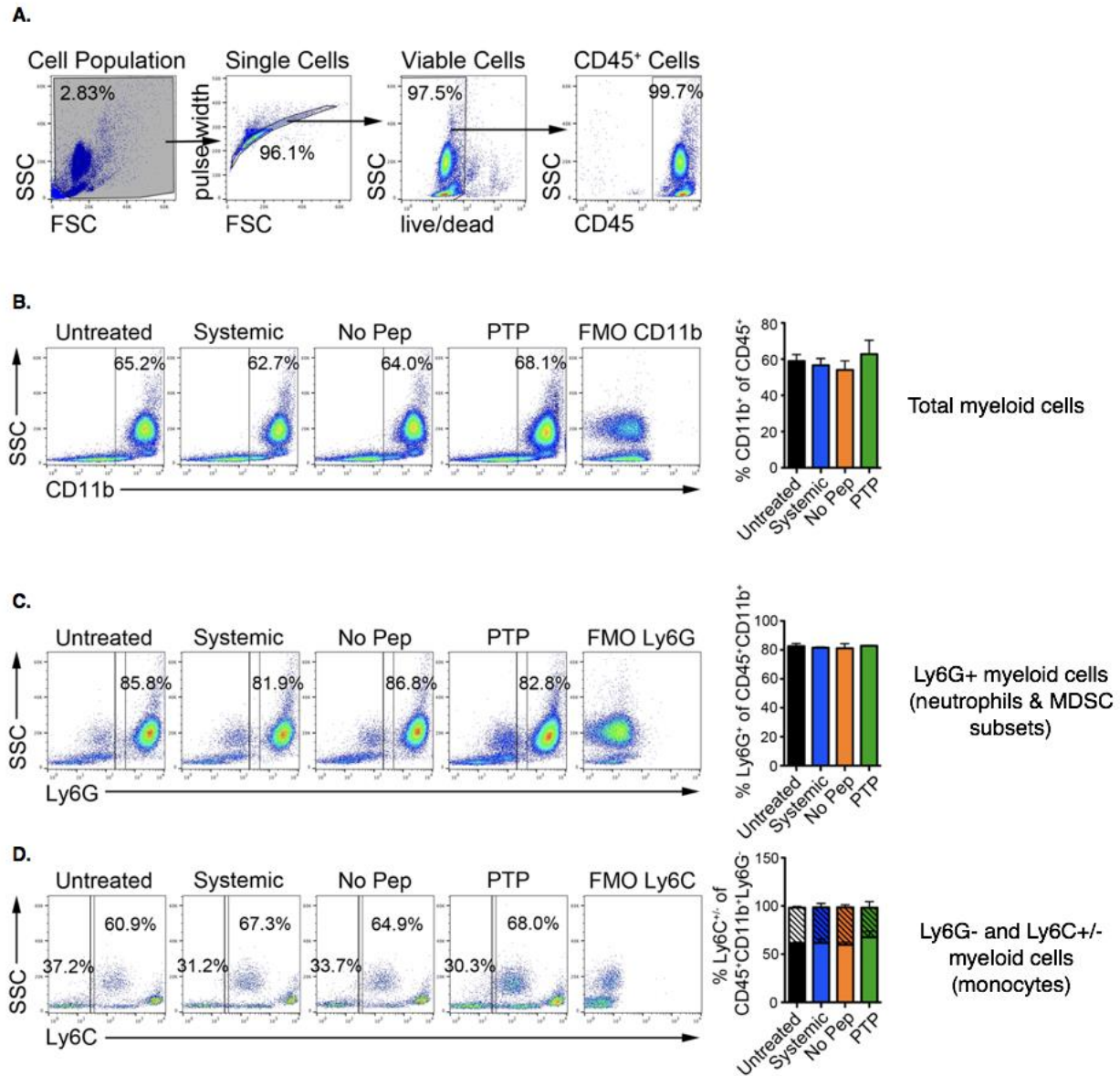


**Figure S16. Myeloid cell populations are not altered with AZ7379 treatment.** (A) Flow cytometry gating scheme utilized to identify the CD45<sup>+</sup> blood leukocyte population. (B) Dot plots represent the percentage of CD11b<sup>+</sup> cells in the CD45<sup>+</sup> cell population. (C) Dot plots represent the percentage of Ly6G<sup>+</sup> cells in the CD45<sup>+</sup>CD11b<sup>+</sup> population. (D) Dot plots represent the percentage of Ly6C<sup>+</sup> and Ly6C<sup>-</sup> monocytes in the CD45<sup>+</sup>CD11b<sup>+</sup>Ly6G<sup>-</sup> population. The percentage of Ly6C<sup>+</sup> (solid) and Ly6C<sup>-</sup> (hashed) cell populations are presented in the bar graph. N=3 mice/treatment. All bar graphs represent the mean  $\pm$  SD.

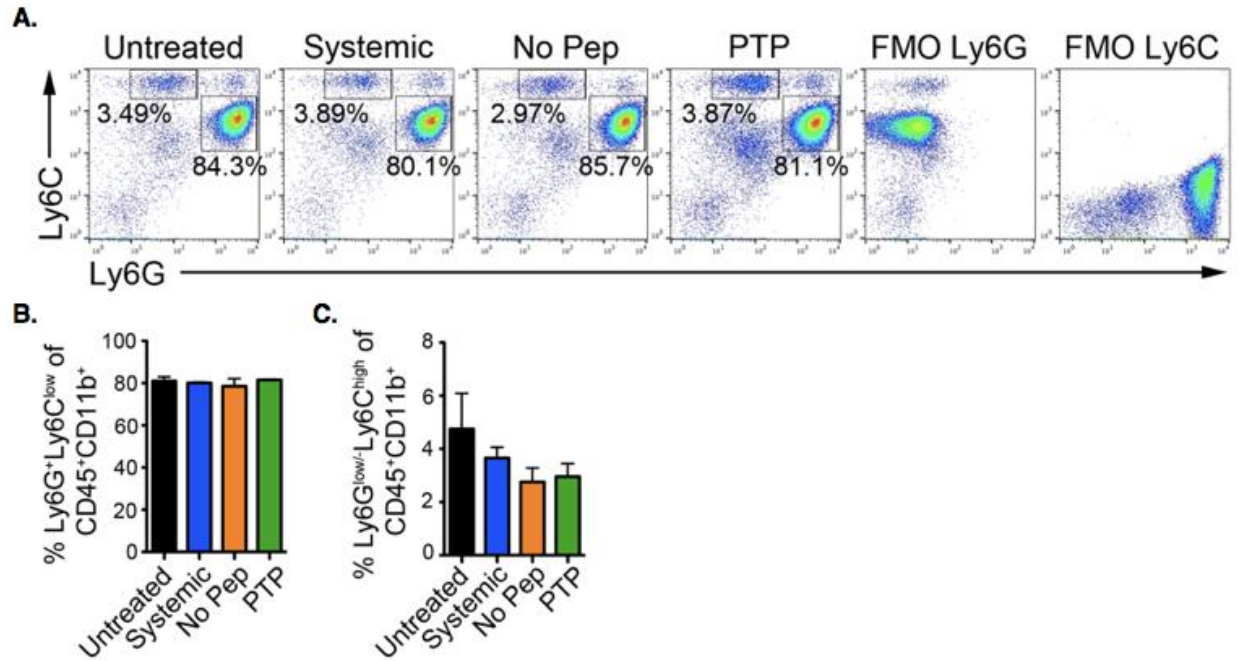


**Figure S17. Myeloid derived suppressor cell populations are not altered in response to AZ7379. (A)** Gating schema for determining myeloid derived suppressor cell in the CD45+CD11b+ blood leukocyte population. **(B)** Granulocytic myeloid derived suppressor cells (GMDSCs) (Ly6C<sup>low</sup> Ly6G<sup>+</sup> of CD45+CD11b+) were similar across all treatment conditions. **(C)** Monocytic myeloid derived suppressor cells (MMDSCs) (bottom right), although not significant, displayed a decreasing trend with liposomal AZ7379, suggestive of reduced immune suppression by MDSCs.